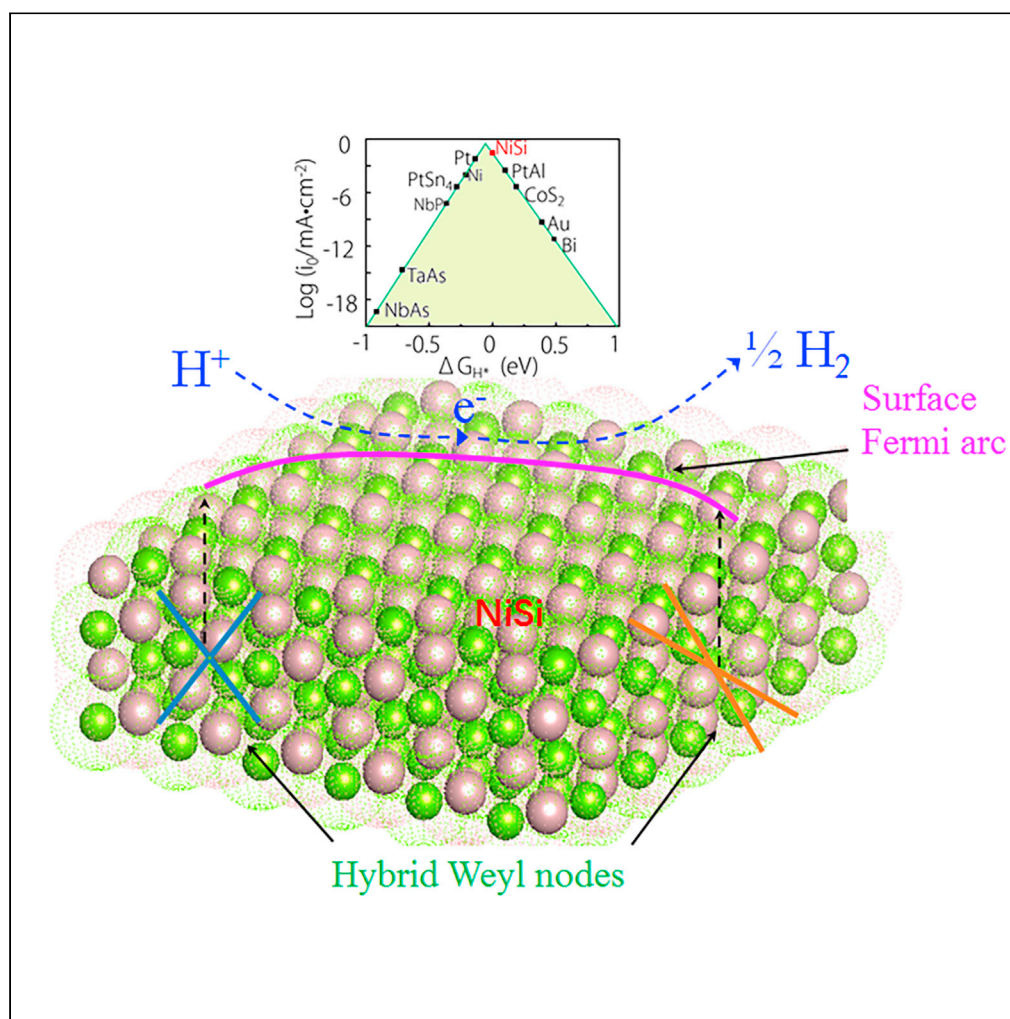


Article

Theoretical realization of hybrid Weyl state and associated high catalytic performance for hydrogen evolution in NiSi



Wei Liu, Xiaoming Zhang, Weizhen Meng, Ying Liu, Xuefang Dai, Guodong Liu

zhangxiaoming87@hebut.edu.cn (X.Z.)
gdlIU1978@126.com (G.L.)

Highlights
A new designation to catalytic enhancement via topological engineering is constructed

An ideal hybrid Weyl catalyst NiSi is identified by a high-throughput material screening

Sufficient evidences verify topological charge participates in catalytic enhancement

NiSi has a higher theoretical hydrogen evolution activity than precious-metal Pt

Liu et al., iScience 25, 103543
January 21, 2022 © 2021 The Authors.
<https://doi.org/10.1016/j.isci.2021.103543>



Article

Theoretical realization of hybrid Weyl state and associated high catalytic performance for hydrogen evolution in NiSi

Wei Liu,^{1,2} Xiaoming Zhang,^{1,2,3,*} Weizhen Meng,^{1,2} Ying Liu,¹ Xuefang Dai,¹ and Guodong Liu^{1,2,*}

SUMMARY

For electrochemical hydrogen evolution reaction (HER), developing high-performance catalysts without containing precious metals have been a major research focus in the present. Herein, we show the feasibility of HER catalytic enhancement in Ni-based materials based on topological engineering from hybrid Weyl states. Via a high-throughput computational screening from ~140,000 materials, we identify that a chiral compound NiSi is a hybrid Weyl semimetal (WSM) showing bulk type-I and type-II Weyl nodes and long surface Fermi arcs near the Fermi level. Sufficient evidences verify that topological charge carriers participate in the HER process, and make the certain surface of NiSi highly active with the Gibbs free energy nearly zero (0.07 eV), which is even lower than Pt and locates on the top of the volcano plots. This work opens up a new routine to develop no-precious-metal-containing HER catalysts via topological engineering, rather than traditional defect engineering, doping engineering, or strain engineering.

INTRODUCTION

Rapid global energy consumption has been seen because of explosion of urbanization and industrialization in today's world. During the production of energy, the overdependence on fossil fuels has induced overmuch carbon emission and the associated environmental degradation (Obama, 2017). Facing on these issues, much effort has been made on developing green energy carriers (Seh et al., 2017; Ding et al., 2019). Among them, hydrogen has been hoped for the most as the alternative carrier to fossil fuels for future electric powering (Mahmood et al., 2018; Wang et al., 2009; Turner, 2004). Until now, various methods have been proposed for hydrogen production, of which water electrolysis is viewed as an effective approach (Eljack and Kazi, 2021; Kalamaras and Efstratiou, 2013; Tiwari et al., 2018; Carvalho et al., 2020). Fundamental mechanism on electrochemical hydrogen evolution reaction (HER) has already been well demonstrated, and has also played an important platform to understand other heterogeneous reactions (Turner, 2004; Wang et al., 2009; Nørskov et al., 2005). Especially, the well-known volcano plots have been set up, which can soundly describe the surface catalytic activity in transition metal-based catalysts for HER process. On volcano plots, precious-metal Pt nearly locates on the mountaintop with hosting the most profitable Gibbs free energy (ΔG_{H^+}) (Seh et al., 2017; Greeley et al., 2006; Ma et al., 2019). However, the utilization of Pt is largely limited by its significantly high cost for large-scale hydrogen production. For this reason, exploring high-efficiency catalysts based on cheaper transition metals such as Ni are highly desirable. Nevertheless, Ni fundamentally has a larger $|\Delta G_{H^+}|$ than Pt (0.22 eV versus 0.09 eV) (Greeley et al., 2006). Various approaches such as chemical doping, phase engineering, and defect engineering have been tried to speed up the surface catalytic activity in Ni (Chhetria et al., 2017; Escalera-Lopez et al., 2016; Adán et al., 2012; Wang et al., 2018). Much progress is obtained under these attempts, but Ni-based catalysts still have much disparity comparing with Pt. Beside the experimental attempts, high-throughput computation has also been applied to explore high-performance catalysts (Di et al., 2018; Handoko et al., 2018; Lim et al., 2020; Wang et al., 2021a, 2021b).

Since the establishment of topological framework, the field of condensed matter physics has undergone a revolutionary innovation. Starting from the earliest reported topological insulators (Hasan and Kane, 2010; Qi and Zhang, 2010), topological semimetals with Weyl/Driac nodes, various nodal lines, and nodal surface have gradually become the focus of current research (Chiu et al., 2016; Bansil et al., 2016; Armitage et al., 2018; Wan et al., 2011; Weng et al., 2015; Yang et al., 2014; Zhang et al., 2018a, 2018b; Wu et al., 2018a, 2018b; He et al., 2020,

¹State Key Laboratory of Reliability and Intelligence of Electrical Equipment, Hebei University of Technology, Tianjin 300130, China

²School of Materials Science and Engineering, Hebei University of Technology, Tianjin 300130, China

³Lead contact

*Correspondence:
zhangxiaoming8@hebut.edu.cn (X.Z.),
gdlIU1978@126.com (G.L.)
<https://doi.org/10.1016/j.isci.2021.103543>



2021a, 2021b; Jin et al., 2020; Wang et al., 2021a, 2021b). The application of topological materials has been rapidly expanded owing to their unique physical properties and electronic characteristic (Moore, 2010; Ren et al., 2016). Especially, it has been demonstrated recently that metallic surface states in topological materials could favor heterogeneous catalysis (Xiao et al., 2015; Chen et al., 2011). Such metallic surface states for catalysis speed-up include Dirac ones in topological insulator, Fermi arc ones in Weyl/Dirac semimetals, and drumhead ones in nodal line semimetals, as evidenced in tens of topological materials by both theoretical and experimental investigations (Chen et al., 2011; Xiao et al., 2015; Rajamathi et al., 2017; Zhang et al., 2018a, 2018b; Li et al., 2018a, 2018b, 2019a, 2019b, 2019c; Yang et al., 2021). Such phenomenon inspired us with the following question: can the Ni-based materials be combined with the novel physical features related to the topologically nontrivial surface states to enhance the activity in HER process?

To pursue this question, herein, we carry out topological engineering in Ni-based materials toward high-efficiency HER catalysts. We first build up the designing scheme, which highlights hybrid Weyl semimetals (WSMs) with different types of Weyl nodes and long surface Fermi arcs which are the ideal material platform for the target. Then, we perform high-throughput material screening to explore concrete examples for Ni-based hybrid WSMs. Further, the identified material NiSi is theoretically demonstrated to show hybrid Weyl nodes, long surface Fermi arcs, and a nearly zero ΔG_{H^+} , suggesting excellent prospect as high-efficiency HER catalysts. The nontrivial band topology and the associated long Fermi arcs on the surface are evidenced to be responsible for the high HER activity in NiSi. This work highly promises topological engineering being a feasible approach to realize high-performance catalysts without involving precious metals.

Designing scheme

Among various topological HER catalysts proposed previously (Chen et al., 2011; Xiao et al., 2015; Rajamathi et al., 2017; Zhang et al., 2018a, 2018b; Li et al., 2018a, 2018b, 2019a, 2019b, 2019c; Yang et al., 2021), WSMs have been one of the most remarkable categories, where the surface Fermi arcs originating from bulk Weyl nodes are believed to enhance catalytic activity by providing robust active center, high carrier density, and mobility around the Fermi energy (Rajamathi et al., 2017). The situation seems wonderful! Unfortunately, it seems that the catalytic enhancement in existing WSMs only works in a finite level, which is largely because that the length of Fermi arcs in traditional WSMs is usually very short. Thus, this designing scheme aims at developing WSMs with long surface Fermi arcs.

Then, how to realize long Fermi arcs in WSMs? Considering the tilting degree of the Weyl cone in the momentum space, Weyl nodes can be classified as two typical categories (i.e. type-I and type-II) (Soluyanov et al., 2015; Chang et al., 2017). As shown in Figures 1A and 1B, Type-I and type-II Weyl nodes show conventional and totally tilted band crossing, respectively. For WSMs contains only one type (either type-I or type-II) of Weyl nodes, long surface Fermi arcs are less likely to appear because the pairs of Weyl nodes with opposite charities are axisymmetrical distributed (assuming that the system preserves the time-reversal symmetry and only contains few pairs of Weyl nodes). However, the situation will change if type-I and type-II of Weyl nodes coexist in a single WSM, as shown by the case in Figure 1C. In this case, type-I and type-II of Weyl nodes happen in different k-paths (also usually locating at different energy levels); thus, the Fermi arcs which connect these Weyl nodes in principle need to span a large area on the surface. In fact, such novel WSM with hosting both type-I and type-II Weyl nodes has already proposed in model in 2016, defined as hybrid WSM (Li et al., 2016). Figure 1D shows the catalytic mechanism for a hybrid WSM. The figure has indicated the presence of type-I and type-II Weyl nodes in the bulk, which generate long Fermi arc on the surface and the associated high surface electron density of states (DOSs).

To testify above assumption, the most crucial determination lies in identifying hybrid WSM candidate in Ni-based compounds. This is a challenging task, noticing that excellent hybrid WSMs are quite rare, which were only identified in few materials including T_d -MoTe₂, OsC₂, YCoC₂, and HfCuP (Xu et al., 2018, 2019; Zhang et al., 2018a, 2018b; Meng et al., 2020a, 2020b). On considering this fact, we make a high-throughput material screening based on Material Project (Jain et al., 2013) (with ~140,000 entries). We show the computational screening process in Figure 2. For the first step, we screen out the materials under chiral space groups from Materials Project data, after which the number of candidates has been sharpened down to 17,928. Then, we exclude chiral compounds without containing Ni element, which results in 858 compounds. Further, we exclude insulating chiral Ni-based compounds by assessing band gap, and metallic ones are retained for further computation. For the next step, we carry out band-structure calculations for detecting potential band crossings, which are essential for WSMs. Only the band crossings within |

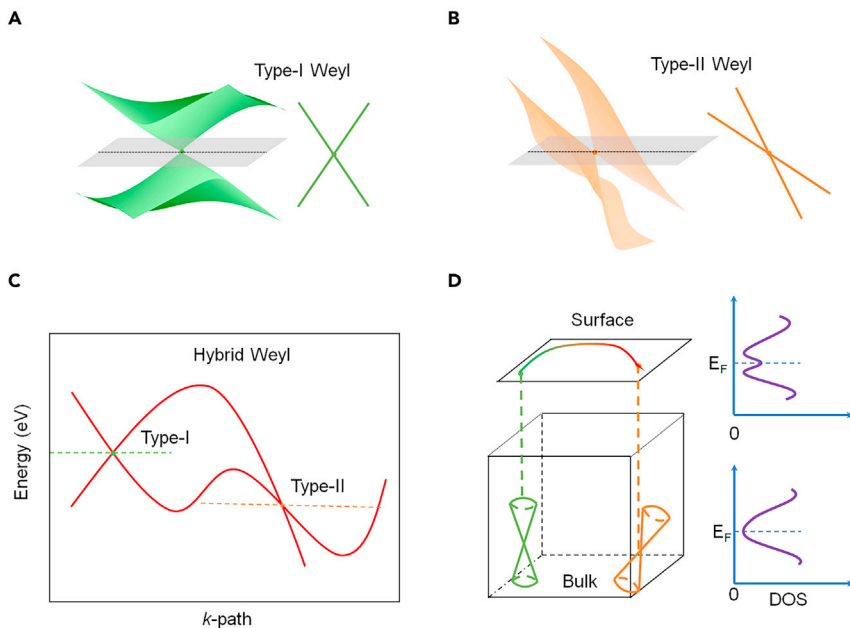


Figure 1. The models for Weyl points and surface states

(A and B) 3D and 2D band dispersion model for (A) type-I and (B) type-II Weyl points.

(C) Illustration of hybrid nodal points composed by one type-I and one type-II Weyl point.

(D) Schematic of hybrid Weyl points in the bulk (left lower panel) and associated long Fermi arc on the surface (left upper panel). The DOSs for the bulk Weyl points and surface Fermi arc are provided in right panels.

$E - E_F < 0.1$ eV are taken into account, because the electrons in this region are the most likely to contribute the conducting nature of the material. Furthermore, we identify the nature of the band crossings, and the final candidate materials need to contain both type-I and type-II Weyl nodes. During material screening, we fortunately find compound NiSi can satisfy all the rigorous screening standards. Thus, in the following, we systematically investigate the topological feature and catalytic performance for HER.

RESULTS

Crystal structure and band topology of NiSi

Until now, many Ni-Si binary phases with different compositions including Ni_2Si , NiSi , and NiSi_2 have been synthesized by solid-state reaction between Ni and Si below their eutectic temperature (Julies et al., 1999). For NiSi compound with the 1:1 stoichiometry, six experimentally synthesized phases under orthorhombic, hexagonal, tetragonal, and also cubic structure were reported in literatures (Julies et al., 1999; Boren, 1933; Osawa and Okamoto, 1939; Pauling and Soldate, 1948; Toman, 1951; Dahal et al., 2016; Kim and Anderson, 2005; Baeri et al., 1989; Sidorenko et al., 2008). These phases were evidenced to be stable with pressure below 300 GPa (Wood et al., 2013). The orthorhombic NiSi within the MnP-type structure (with the space group $Pnma$) was determined to be the most stable phase at the atmospheric pressure. This structure can be viewed as the distorted hexagonal NiAs-type structure, where both Ni and Si atoms are assigned within six-fold coordination. This NiSi phase has been synthesized by different approaches such as arc-melting, sputtering, and Czochralski pulling technique (Dobson et al., 2016; Detavernier et al., 2003; Meyer et al., 1997). Besides, under the pressure about 23 GPa, NiSi with the tetragonal CuTi-type structure ($P4/nmm$, B11) can be prepared. At higher pressures, four other NiSi phases under two orthorhombic structures (the $Pbma$ -I one and the $Pnma$ FeB structure) and two cubic ones (the CsCl-type structure and the ϵ -FeSi structure) were also observed stable. NiSi focused in this work is one of the cubic phases taking the ϵ -FeSi structure. The structure belongs to the chiral space group $P213$ (No.198). This NiSi phase has been successfully synthesized by different methods previously (Julies et al., 1999; Boren, 1933; Baeri et al., 1989; Sidorenko et al., 2008). Most remarkably, Saeri et al. reported the epitaxial preparation of NiSi on the (111) Si substrates (Baeri et al., 1989). They found that cubic NiSi with ϵ -FeSi structure would appear by the melting from the pulsed laser irradiation of the epitaxial NiSi films. Under this approach, cubic NiSi usually coexists with the orthorhombic phase; then, the preparation of large-area and

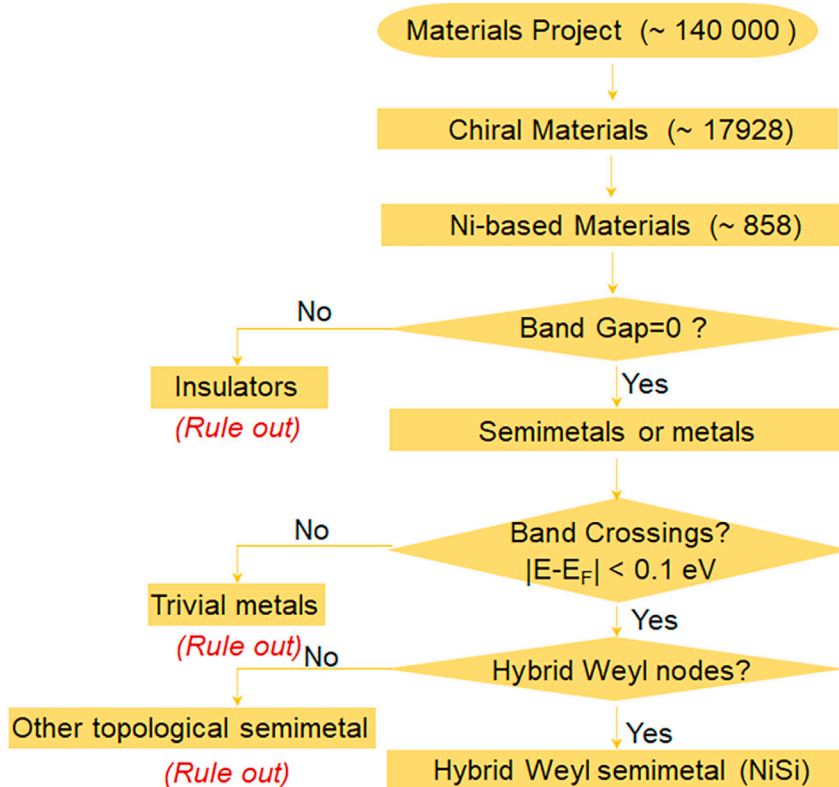
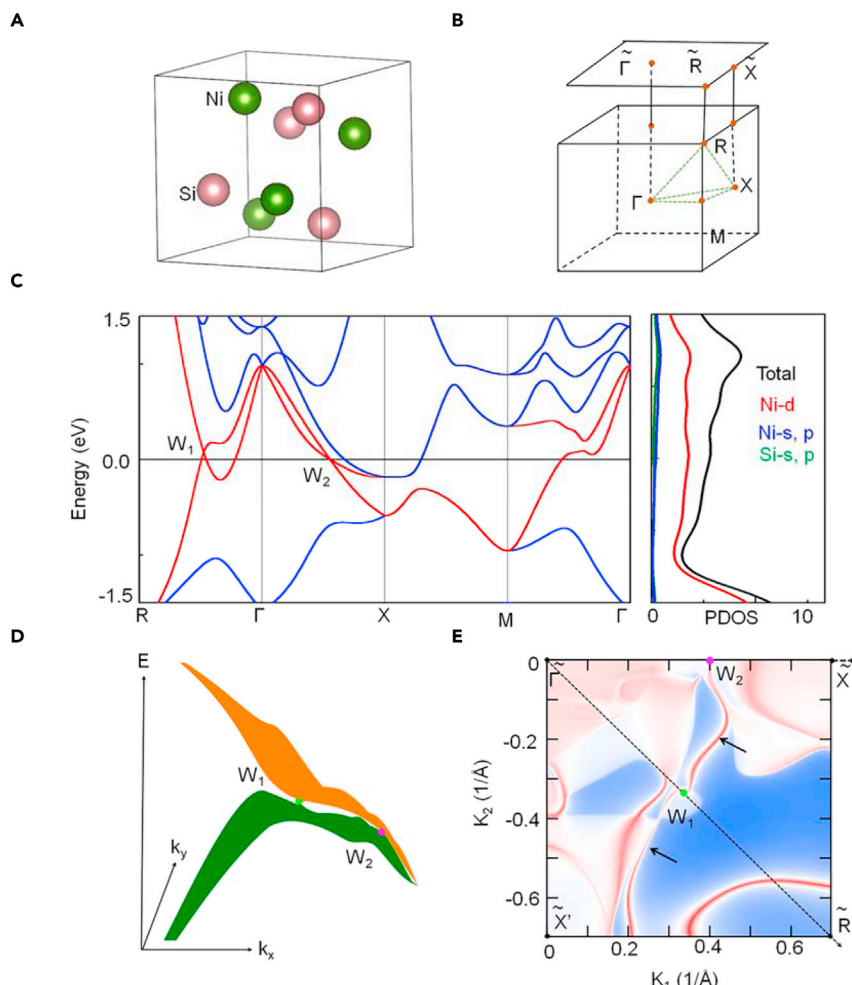


Figure 2. Flowchart of high-throughput computational screening for Ni-based hybrid Weyl semimetal from the Materials Project database

homogeneous NiSi could be a challenge, where the irradiation time and the subsequent annealing process are very crucial. Later, Julies *et al.* developed the direct preparation of epitaxial NiSi with ϵ -FeSi structure by successfully controlling the diffusion of Ni into the Si substrate (Julies *et al.*, 1999); however, during this process the epitaxial temperature and the annealing condition need to be carefully treated because the ϵ -FeSi phase of NiSi is less stable than the orthorhombic phase.

The atomic lattice structure of ϵ -FeSi-type NiSi is shown in Figure 3A. One NiSi unit cell contains 4 Ni and 4 Si atoms. The atoms are arranged in the distorted face-centered cubic structure, where the Ni atoms are forced out from their original positions by the Si atoms. The optimized lattice constant for NiSi is $a = b = c = 4.496 \text{ \AA}$, being comparable with experimental one (4.437 \AA) (Boren, 1933). We calculated the band structure and the electronic DOSs of NiSi (Figure 3C). Two Weyl nodes (remarked as W_1 and W_2) can be observed near the Fermi level, where W_1 situates at 0.079 eV above the Fermi level locating on the k -path $R-\Gamma$ while W_2 locates at 0.005 eV on the $\Gamma-X$ path. The provided DOSs indicates the conducting electronic states are almost contributed by the $3d$ orbitals of the Ni atom. The Weyl nodes manifest different band slopes where W_1 is a type-I Weyl node while W_2 is type-II. These Weyl nodes are formed by the intersections between the same two bands, which can be clearly observed by the 3D plotting of the bands (Figure 3D). Thus, NiSi compound can be well characterized as a hybrid WSM. We take the (001) surface projection to investigate the surface states of NiSi compound (Figure 3B). We show the slice of surface states at the Fermi energy (Figure 3E). Considering the C_4 symmetry in the system, the slice range is only selected as 1/4 of the whole surface Brillouin region. We indeed observe long Fermi arcs corresponding to Weyl nodes W_1 and W_2 , where the extension of Fermi arcs spans most region of the slice, as shown in Figure 3C.

The spin-orbit coupling (SOC) cannot be simply ignored in NiSi. Thus, in the following, we discuss the electronic band with taking into account SOC. As shown in Figure 4A, we find the bands experience slight split under SOC. Still, we pay special attention to the bands in the $R-\Gamma$ and $\Gamma-X$ paths (remarked as region I and II). The enlarged band structures for them are shown in Figure 4B. We find the Weyl nodes in NiSi are

**Figure 3. Cyrstal structure and electronic structure without SOC**

- (A) Atomic lattice structure of NiSi compound.
- (B) The bulk and the (001) surface Brillouin zone with high-symmetry k -points provided.
- (C) Electronic band structure projected density of states (PDOSs) of NiSi compound. The two band crossings in the band structure are denoted as W_1 and W_2 .
- (D) 3D plotting of band dispersions for the hybrid Weyl nodes.
- (E) The constant energy slices corresponding to (001) surface at the Fermi level. The Fermi arcs are pointed by the arrows.

multiplied under SOC, where two type-I Weyl nodes (W_3 and W_4) appear in the $R-\Gamma$ path and two type-II ones (W_5 and W_6) in $\Gamma-X$ path. These results indicate NiSi is still a hybrid WSM under SOC. To give more convinced results, we have also rechecked the electronic band structure under SOC from the Heyd–Scuse–Ria–Ernzerhof (HSE) functional (Heyd et al., 2003), as shown Figure S1. We can find that the Weyl nodes in the $R-\Gamma$ and $\Gamma-X$ path retain under the HSE + SOC calculations. Then, we investigate the surface states under SOC. The (001) surface band structure is shown in Figure 4C, where the Fermi arcs from the Weyl nodes can be clearly identified. Furthermore, we display the slice of surface states at the Fermi energy (Figure 4D). We find these long Fermi arcs almost transverse the entire slice space.

HER performance of NiSi

With the hybrid Weyl natural and the existence of long surface Fermi arcs in minds, we continue to investigate the HER catalytic performance in NiSi compound. The possible HER catalytic mechanism in NiSi is schematically shown in Figure 5A. The hybrid Weyl nodes bring long Fermi arcs on the (001) surface of NiSi, which makes the surface with high activity and spires the HER process by reducing the ΔG_{H^+} and increasing the surface conductivity. We simulate the HER process by adsorbing single H atom on the NiSi slab with the Ni-terminated (001)

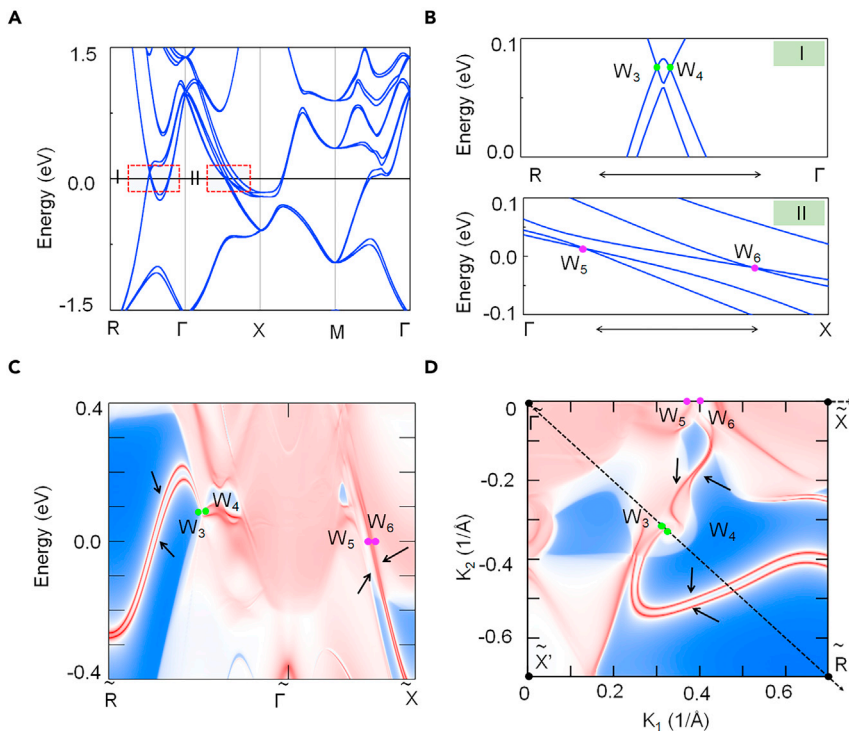


Figure 4. Electronic structure under SOC

(A) Electronic band structure of NiSi compound with SOC included. The band crossings near the Fermi level are highlighted by two regions (I and II in the figure).

(B) Enlarged band structure for region I and region II. The four Weyl points are denoted as W_3 - W_6 .

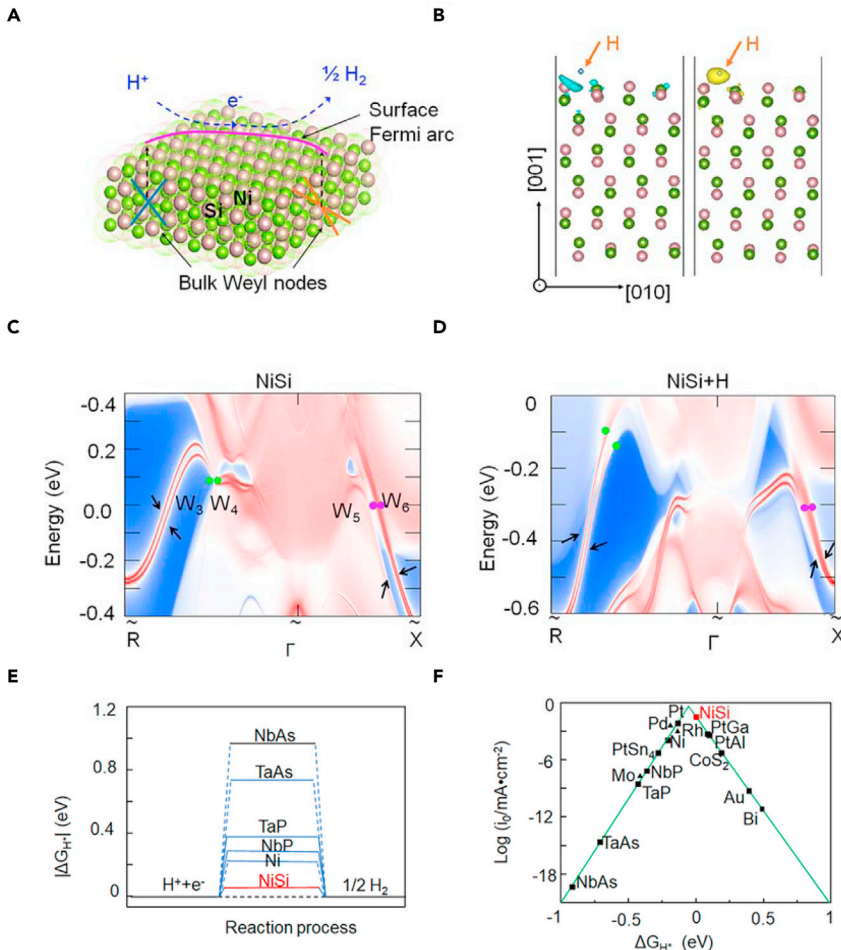
(C) Projected spectrum on the (001) surface of NiSi. The positions of the projected hybrid Weyl points and Fermi arcs are shown by the dot and arrow, respectively.

(D) The constant energy slices corresponding to (010) surface at the Fermi level.

surface. Our calculations show the most favorable adsorption site for H is on the top of Ni atom. Under this state, we provide the map of the charge density difference (Figure 5B). We find sizable charge depletion on the (001) surface of NiSi (see the left panel), which has transferred to H adatom (i.e. charge accumulation on H, see the right panel). The charge accumulation on H atom arises from the fact that the electronegativity of H is higher than that of Ni. Besides, the case for the adsorption of molecular hydrogen (H_2) on NiSi surface is also considered (the corresponding kinetic process will be discussed later). For this case, we can still observe a small amount of charge exchange between NiSi and H_2 (see Figure S2).

In addition, in Figures 5C and 5D, we compare the surface band structure of NiSi before and after H adsorption. It can be clearly seen that the four Weyl node points move down after adding H atoms on the NiSi surface, indicating that the charge transfer takes place on its surface. We find the Fermi arcs moves toward lower energy after H adsorption, further verifying the charge exchange between NiSi surface and H atom during the HER process.

The HER activity in NiSi can be directly reflected by ΔG_{H^*} . Just as expected, the calculated ΔG_{H^*} is close to zero (0.077 eV). We compare the HER activity between NiSi and Weyl HER catalysts proposed before (Figure 5E). For comparison, the case of pure Ni is also provided. We find $|\Delta G_{H^*}|$ of NiSi (0.07 eV) is significantly lower than WSMs NbAs (0.96 eV), TaAs (0.74 eV), TaP (0.38 eV), and NbP (0.31 eV) (Rajamathi et al., 2017), and Ni (0.22 eV) as well (Greeley et al., 2006). The relatively low ΔG_{H^*} benefits from the long surface Fermi arcs in NiSi. Furthermore, we show the volcano curves in Figure 5F. We can observe that NiSi almost locates at the top of the volcano curves. Remarkably, by only view on the ΔG_{H^*} , the HER activity in NiSi is even better than the precious Pt (0.07 eV v.s. 0.09 eV) (Greeley et al., 2006). Furthermore, we estimate the kinetics of the HER reaction in NiSi. Two possible elementary reactions including the Heyrovsky reaction (H-reaction) and the Tafel reaction (T-reaction) are considered. The reaction barrier is estimated by using the climbing image-nudged

**Figure 5. HER process and Volcano plot**

(A) Schematic illustration of the HER process on the (001) surface with the enhanced activity by the hybrid Weyl nodes induced long Fermi arcs.

(B) The electron depletion (the left pannel) and accumulation (the right panel) during H adsorption on NiSi (001) surface. The isosurface is taken as 0.005 electrons/ \AA^3 .

(C and D) show the (001) surface states of NiSi before and after the hydrogen adsorption, respectively.

(E) The free-energy diagram for hydrogen evolution for NiSi and typical catalysts. The case of Ni is also provided for comparison. The data for NbAs, TaAs, NbP, and TaP are taken from (Rajamathi et al., 2017). The data for PtSn₄ is taken from (Li et al., 2019a, 2019b, 2019c). The data for Ni is taken from (Ma et al., 2019).

(F) Volcano plot for HER of NiSi in comparison with typical catalysts. Except NiSi, the data for other catalysts are taken from (Ma et al., 2019; Chen et al., 2011; Xiao et al., 2015; Rajamathi et al., 2017; Zhang et al., 2018a, 2018b; Li et al., 2018a, 2018b, 2019a, 2019b, 2019c; Yang et al., 2021; Soluyanov et al., 2015).

elastic band (CI-NEB) method (Henkelman et al., 2000). The results show the T-reaction barrier is much lower (see Figure S3), suggesting the HER process is more possible to go through the T-reaction route. Especially, the barrier for the T-reaction in NiSi is as low as 0.48 eV, being close to the modified MXenes and precious-metal-containing catalysts (Li et al., 2018a, 2018b; Skúlason et al., 2007). Besides, for electrocatalysts, the HER performance also highly relates to the position of Fermi level with respect to the HER potential. Our calculation shows NiSi has a good energy-level matching for excellent electrocatalytic activity with the Fermi level situating at 0.23 eV above the HER potential. Together with the relatively low ΔG_{H^*} , the hybrid WSM NiSi is promising to serve as a superior HER catalyst without containing precious-metal elements.

To fully ascertain the relationship between the hybrid Weyl nodes and the HER activity, we artificially tune the positions of the hybrid Weyl nodes by different approaches. As the first, we perform hydrostatic distortions to the NiSi lattice. In Figure 6A, we show the positions of the hybrid Weyl nodes (W_1 and W_2) under

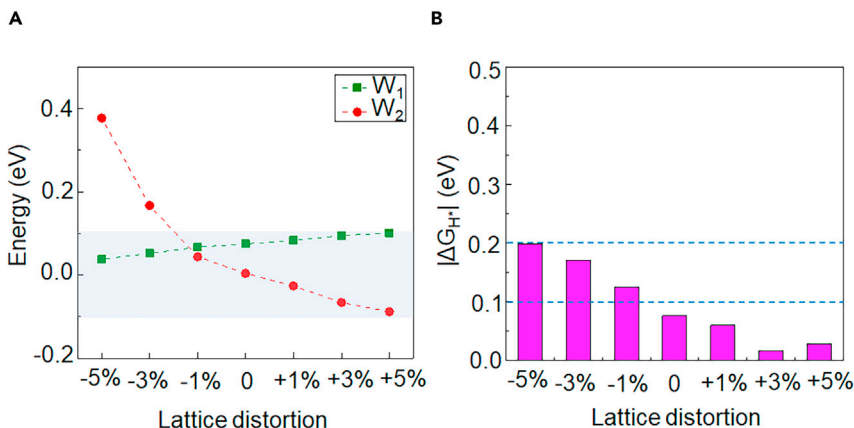


Figure 6. Tuning the Weyl nodes and HER performance by strain

(A) The positions of the hybrid Weyl nodes (W_1 and W_2) under hydrostatic lattice distortions from -5% to $+5\%$, where negative and positive values represent lattice compression and lattice expansion, respectively.

(B) The calculated $|\Delta G_{H^*}|$ on the (001) surface of NiSi under hydrostatic lattice distortions from -5% to $+5\%$.

hydrostatic lattice distortions from -5% to $+5\%$, where negative and positive values represent lattice compression and lattice expansion, respectively. One can find that the position of W_1 does not change much during lattice distortions, which almost retains in the energy range of ± 0.1 eV. For comparison, the position of W_2 experiences greater changes, especially under lattice compression. Notably, as shown by the shadowed region in Figure 6A, both W_1 and W_2 locate quite near the Fermi level (within $|E - E_F| < 0.1$ eV) at most lattice distortions. This indicates hybrid Weyl nodes and the surface Fermi arcs in NiSi are weakly sensitive to the lattice distortions. Correspondingly, the high (001) surface HER activity is expected to retain as well. This expectation has been verified by our calculations. As shown in Figure 6B, the calculated $|\Delta G_{H^*}|$ on the (001) surface for all the cases are below 0.2 eV, suggesting high HER activity in NiSi. These results suggest the HER activity is highly relative to the hybrid Weyl nodes in NiSi.

Because the hybrid Weyl nodes are weakly sensitive to lattice distortions, here, we further tune the hybrid Weyl nodes by artificially shifting the number of electrons (NE.) in NiSi system. Here, we want to point out that, this is only a theoretical treatment because the total number of electrons for NiSi is definite without doping or defects. However, this can be easily realized from the theoretical VASP package. As shown in Figures 7A–7C, such treatment can not only ensure the presence of hybrid Weyl nodes but also can effectively tune the position of these Weyl nodes. As shown by the band structure in Figure 7A, both the type-I and type-II Weyl nodes will move to high energy levels (at about 0.3 eV–0.4 eV) when NiSi system loses one electron. On the contrary, the Weyl nodes will be pulled into low energy levels (at about -0.3 eV) when NiSi system gains one electron, as shown in Figure 7C. For comparison, the band structure for native NiSi is provided in Figure 7B, where the Weyl nodes locate quite near the Fermi level (W_1 at 0.079 eV and W_2 at 0.005 eV). Comparing with native NiSi (NE. = 80), the hybrid Weyl nodes and corresponding surface Fermi arcs for the cases with losing one electron (NE. = 79) and gaining one electron (NE. = 81) are expected to be less contributing to the HER process, because the Weyl nodes in these cases are far away from the Fermi level. In Figure 7D, we compare the $|\Delta G_{H^*}|$ on the (001) surface of NiSi with NE. = 79, 80, and 81. The results show that, with tuning the Weyl nodes away from the Fermi level, $|\Delta G_{H^*}|$ for NiSi system indeed greatly increase (3.89 eV for Nelec. = 79, and 3.24 eV for Nelec. = 81), suggesting the weakness of HER activity during the period. These results have fully revealed the strong relation between HER activity and hybrid Weyl nodes in NiSi.

Before closing, we have several remarks. First, we come to aware that a recent work already observed good HER catalytic performance of NiSi in experiments, along with several other transition-metal monosilicides (namely MSi, M = Ti, Mn, Fe, Ru, Ni, Pd, Co, and Rh) (He et al., 2021a, 2021b). Their experiments showed all explored MSi electrodes have low overpotentials with favorable Tafel slopes, which are even comparable to that of the commercial 20 wt% Pt/C. They argued that the good performance in MSi may arise from the smooth of the M d-orbitals near the Fermi level by the neighboring Si atoms. Such smooth can also be observed from the projected density of states (PDOSs) of NiSi in our study (see Figure 3C). More importantly, in this work, we further clarify the deep origin of the good HER catalytic performance in NiSi from

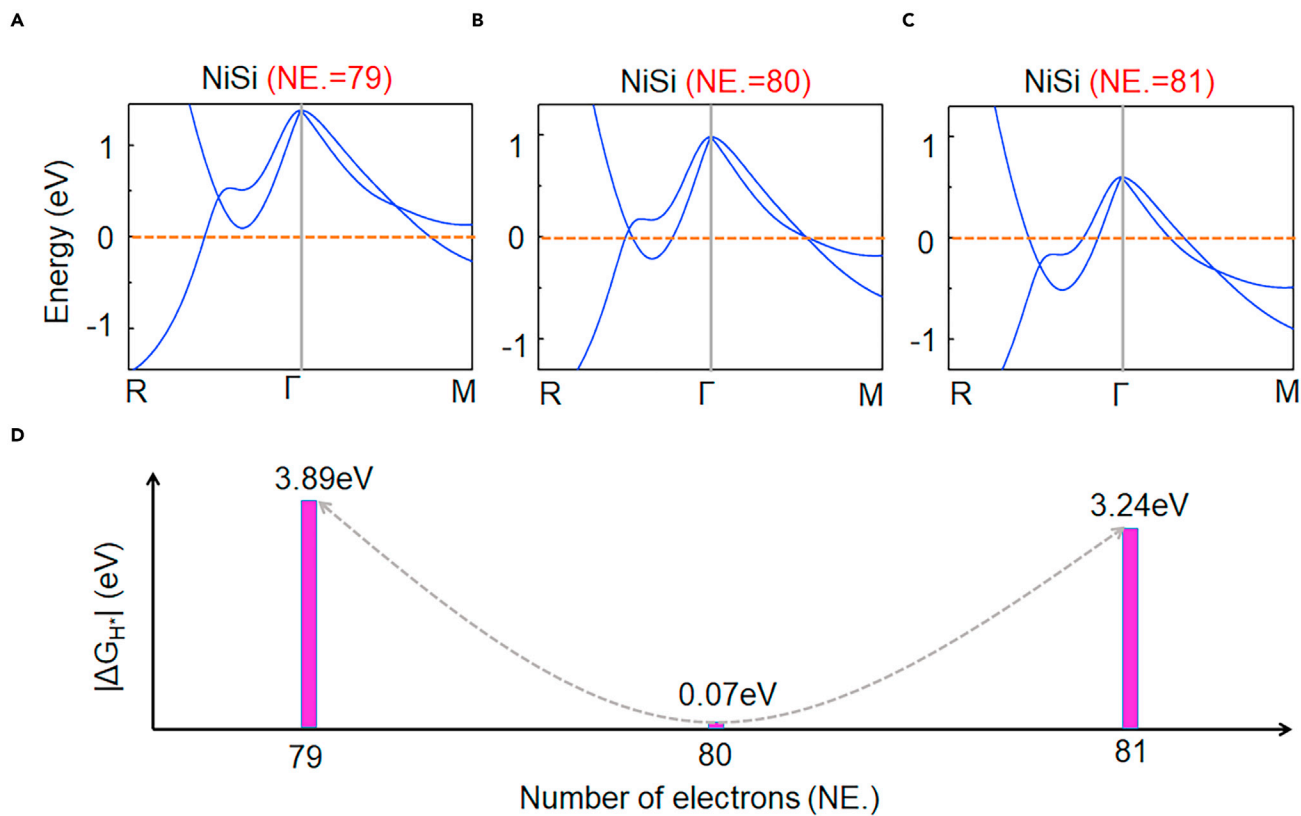


Figure 7. Tuning the Weyl nodes and HER performance by electron/hole doping

(A) Electronic band structure of NiSi with losing one electron. The native number of electrons (NE.) in a NiSi cell is 80. (B and C) are the band structures for native NiSi (NE. = 80) and that with gaining one electron (NE. = 81), respectively. (D) Comparison of $|\Delta G_{H^*}|$ in NiSi among NE. = 79, 80, and 81.

the topological point of view. We find the hybridization between the Ni and Si atoms form hybrid Weyl states near the Fermi level. The hybrid Weyl nodes produce long Fermi arcs on the surface, which induce the high HER activity in NiSi. In addition, based on the recent experiments (He et al., 2021a, 2021b; Chen et al., 2019), when metal silicides MSi are used as HER catalysts, acidic electrolytes can be applied. For example, it is found that, NiSi catalysts can maintain over 6 h stability in 0.5 H₂SO₄ (aq) electrolyte (He et al., 2021a, 2021b). The high stability in electrolytes favors NiSi as a promising HER catalyst.

Second, we want to point out that, to obtain the catalytic enhancement from the topological surface in NiSi, single crystal sample rather than polycrystalline one is required, because the grain boundaries in the polycrystal would scatter off the topological states. Single crystals are also applied in several experimental works on topological catalysts (Rajamathi et al., 2017; Zhang et al., 2018a, 2018b; Li et al., 2019a, 2019b, 2019c). In addition, even in single crystal, the presence of defects could also affect the catalytic performance, because the topological electronic states in NiSi are calculated from the “perfect” crystal, and the hybrid Weyl nodes are highly relative to the hybridization among atoms and the crystal symmetry in NiSi. As shown in Figure S4, under different defects, NiSi can either show one type of Weyl nodes or no Weyl node. Correspondingly, the $|\Delta G_{H^*}|$ for NiSi with defects is calculated in the range of 0.28 eV–0.79 eV. Therefore, to obtain the best catalytic ability, high-quality single crystal of NiSi is favorable.

For the third remark, we stress that this work focuses on the feasibility of hybrid Weyl semimetals as topological catalysts. Unlike generic Weyl semimetals (either type-I or type-II), hybrid Weyl semimetals compose both types of Weyl nodes and potentially show long topological Fermi arcs on the surfaces. Beside NiSi proposed in this work, we have also evaluated the HER catalytic performance on the few examples of hybrid Weyl semimetals proposed previously, including OsC₂, YCoC₂, and HfCuP (Zhang et al., 2018a, 2018b; Xu et al., 2019; Meng et al., 2020a, 2020b). In these examples, only YCoC₂ can be synthesized in

experiments but the hybrid Weyl nodes in this material situate far away the Fermi level (>0.2 eV). Although the hybrid Weyl nodes in OsC₂ and HfCuP are near the Fermi level, these materials are unfortunately hypothetical. The $|\Delta G_{H^*}|$ is calculated to be 0.39 eV for YCoC₂, 0.04 eV for OsC₂, and 0.07 eV for HfCuP. The low $|\Delta G_{H^*}|$ values in OsC₂ and HfCuP further support our argument that the presence of hybrid Weyl nodes near the Fermi level could favor the HER process. More importantly, comparing with these materials, the NiSi proposed in this work seems to be the best example, because it is not only an existing material but also has a relatively low $|\Delta G_{H^*}|$ (0.07 eV).

Conclusions

In conclusion, we have demonstrated hybrid WSM is a promising platform to enhance catalytic activity for HER, where the long Fermi arc states related to hybrid Weyl nodes make certain surface highly active. We perform high-throughput material screening from $\sim 140,000$ materials within the Material Project database, and fortunately identify a Ni-based compound namely NiSi as a new hybrid WSM with high HER activity. NiSi follows a chiral space group, and manifests both type-I and type-II Weyl nodes near the Fermi level. We further verify that on its surface, where long Fermi arcs from hybrid Weyl nodes present, ΔG_{H^*} for HER process is almost zero (0.07 eV), being favorable for high-efficiency catalyst. Remarkably, the absolute value of ΔG_{H^*} in NiSi is even smaller than Pt (0.07 eV v.s. 0.09 eV), and NiSi almost locates on the top of the volcano curves. This work provides new insight on developing high-efficiency catalyst without precious metals by using hybrid WSMs.

Limitations of the study

Our work theoretically demonstrates the feasibility of hybrid Weyl semimetal as a high-performance catalyst for HER. High-throughput material screening is also performed to identifying candidate materials. However, the experimental investigation on the exact HER catalytic activity needs to be further proceeded.

STAR★METHODS

Detailed methods are provided in the online version of this paper and include the following:

- KEY RESOURCES TABLE
- RESOURCE AVAILABILITY
 - Lead contact
 - Materials availability
 - Data and code availability
- METHOD DETAILS

SUPPLEMENTAL INFORMATION

Supplemental information can be found online at <https://doi.org/10.1016/j.isci.2021.103543>.

ACKNOWLEDGMENTS

This work is supported by National Natural Science Foundation of China (Grants No. 11904074). The work is funded by Science and Technology Project of Hebei Education Department, the Nature Science Foundation of Hebei Province, S&T Program of Hebei (A2021202012), the Overseas Scientists Sponsorship Program by Hebei Province (C20210330). The work is also supported the State Key Laboratory of Reliability and Intelligence of Electrical Equipment (No. EERI_OY2020001), Hebei University of Technology. One of the authors (X.M. Zhang) acknowledges the financial support from Young Elite Scientists Sponsorship Program by Tianjin.

AUTHOR CONTRIBUTIONS

X.Z. conceived the research idea. X.Z. and G.L. supervised the research. W.L. performed the material screening. W.L., W.M., Y.L., and X.D. carried out DFT calculations. All authors contributed to result analysis and paper writing.

DECLARATION OF INTERESTS

The authors declare no competing financial interests.

Received: August 31, 2021

Revised: November 2, 2021

Accepted: November 29, 2021

Published: January 21, 2022

REFERENCES

- Adán, C., Pérez-Alonso, F.J., Rojas, S., Peña, M.A., and Fierro, J.L.G. (2012). Enhancement of electrocatalytic activity towards hydrogen evolution reaction by boron-modified nickel nanoparticles. *Int. J. Hydrogen Energ.* 37, 14984–14991.
- Armitage, N.P., Mele, E.J., and Vishwanath, A. (2018). Weyl and Dirac semimetals in three-dimensional solids. *Rev. Mod. Phys.* 90, 015001.
- Baeri, P., Grimaldi, M.G., and Priolo, F. (1989). Epitaxial NiSi layers on <111>-oriented Si obtained by pulsed laser irradiation. *J. Alloys Compd.* 66, 861.
- Bansil, A., Lin, H., and Das, T. (2016). Colloquium: Topological band theory. *Rev. Mod. Phys.* 88, 021004.
- Blöchl, P.E. (1994). Projector augmented-wave method. *Phys. Rev. B* 50, 17953.
- Boren, B. (1933). Röntgenuntersuchung der Legierungen von Si mit Cr, Mn, Co und Ni. *Ark. Kemi Min. Geol.* 11A, 10.
- Carvalho, O.Q., Adiga, P., Murthy, S.K., Fulton, J.L., Gutiérrez, O.Y., and Stoerzinger, K.A. (2020). Understanding the role of surface heterogeneities in electrosynthesis reactions. *iScience* 23, 101814.
- Chang, T.-R., Xu, S.-Y., Sanchez, D.S., Tsai, W.-F., Huang, S.-M., Chang, G., Hsu, C.-H., Bian, G., Belopolski, I., Yu, Z.-M., et al. (2017). Type-II symmetry-protected topological Dirac semimetals. *Phys. Rev. Lett.* 119, 026404.
- Chen, H., Ai, X., Liu, W., Xie, Z.B., Feng, W.Q., Chen, W., and Zou, X.X. (2019). Promoting subordinate, efficient ruthenium sites with interstitial silicon for Pt-like electrocatalytic activity. *Angew. Chem. Int. Ed.* 58, 11409.
- Chen, H., Zhu, W., Xiao, D., and Zhang, Z. (2011). CO oxidation facilitated by robust surface states on Au-covered topological insulators. *Phys. Rev. Lett.* 107, 056804.
- Chhetria, M., Sultana, S., and Raoa, C.N.R. (2017). Electrocatalytic hydrogen evolution reaction activity comparable to platinum exhibited by the Ni/Ni(OH)₂/graphite electrode. *Proc. Natl. Acad. Sci.* 114, 8986–8990.
- Chiu, C.-K., Teo, J.C.Y., Schnyder, A.P., and Ryu, S. (2016). Classification of topological quantum matter with symmetries. *Rev. Mod. Phys.* 88, 035005.
- Dahal, A., Gunasekera, J., Harringer, L., Singh, D.K., and Singh, D.J. (2016). Metallic nickel silicides: Experiments and theory for NiSi and first principles calculations for other phases. *J. Alloys Compd.* 672, 110–116.
- Detavernier, C., Lavoie, C., and d'Heurle, F.M. (2003). Thermal expansion of the isostructural PtSi and NiSi: Negative expansion coefficient in NiSi and stress effects in thin films. *J. Appl. Phys.* 93, 2510.
- Di, J., Yan, C., Handoko, A.D., She, Z.W., Li, H., and Liu, Z. (2018). Ultrathin two-dimensional materials for photo- and electrocatalytic hydrogen evolution. *Mater. Today* 21, 749–770.
- Ding, S., Hulse, M.J., Pérez-Ramírez, J., and Yan, N. (2019). Transforming energy with single-atom catalysts. *Joule* 3, 2897–2929.
- Dobson, D.P., Hunt, S.A., Ahmed, J., Lord, O.T., Wann, E.T.H., Santangelo, J., Wood, I.G., Vocadlo, L., Walker, A.M., Thomson, A.R., et al. (2016). The phase diagram of NiSi under the conditions of small planetary interiors. *Phys. Earth Planet. 261, 196–206.*
- Eljack, F., and Kazi, M.K. (2021). Prospects and challenges of green hydrogen economy via multi-sector global symbiosis in Qatar. *Front. Sustain.* 1, 612762.
- Escalera-Lopez, D., Niu, Y., Yin, J., Cooke, K., Rees, N.V., and Palmer, R.E. (2016). Enhancement of the hydrogen evolution reaction from Ni-MoS₂ hybrid nanoclusters. *ACS Catal.* 6, 6008–6017.
- Greeley, J., Jaramillo, T.F., Bonde, J., Chorkendorff, I., and Nørskov, J.K. (2006). Computational high-throughput screening of electrocatalytic materials for hydrogen evolution. *Nat. Mater.* 5, 909–913.
- Grimme, S. (2006). Semiempirical GGA-type density functional constructed with a long-range dispersion correction. *Comput. Chem.* 27, 1787–1799.
- Handoko, A.D., Fredrickson, K.D., Anasori, B., Convey, K.W., Johnson, L.R., Gogotsi, Y., Vojvodic, A., and Seh, Z.W. (2018). Tuning the basal plane functionalization of two-dimensional metal carbides (MXenes) to control hydrogen evolution activity. *ACS Appl. Energy Mater.* 1, 173–180.
- Hasan, M.Z., and Kane, C.L. (2010). Colloquium: Topological insulators. *Rev. Mod. Phys.* 82, 3045.
- He, T., Zhang, X., Wang, L., Liu, Y., Dai, X.F., Wang, L., and Liu, G.D. (2021a). Ideal fully spin-polarized type-II nodal line state in half-metals X₂YZ₄ (X=K, Cs, Rb, Cr, Cu, Z=Cl, F). *Mater. Today Phys.* 17, 100360.
- He, T.L., Zhang, X.M., Liu, Y., Dai, X.F., and Liu, G.D. (2020). Ferromagnetic hybrid nodal loop and switchable type-I and type-II Weyl fermions in two dimensions. *Phys. Rev. B* 102, 075133.
- He, Y., Wang, T.-L., Zhang, Man., Wang, T.-W., Wu, L.-F., Zeng, L.Y., Wang, X.P., Boubeche, M., Wang, S., Yan, K., et al. (2021b). Discovery and facile Synthesis of a new silicon based family as efficient hydrogen evolution reaction catalysts: a computational and experimental investigation of metal monosilicides. *Small* 17, 2006153.
- Henkelman, G., Uberuaga, B.P., and Jónsson, H. (2000). A climbing image nudged elastic band method for finding saddle points and minimum energy paths. *J. Chem. Phys.* 113, 9901–9904.
- Heyd, J., Scuseria, G.E., and Ernzerhof, M. (2003). Hybrid functionals based on a screened Coulomb potential. *J. Chem. Phys.* 118, 8207.
- Jain, A., Ong, S.P., Hautier, G., Chen, W., Richards, W.D., Dacek, S., Cholia, S., Gunter, D., Skinner, D., Ceder, G., and Persson, K.A. (2013). Commentary: The Materials Project: A materials genome approach to accelerating materials innovation. *APL Mater.* 1, 011002.
- Jin, L., Zhang, X.M., Liu, Y., Dai, X.F., Shen, X.N., Wang, L.Y., and Liu, G.D. (2020). Two-dimensional Weyl nodal-line semimetal in a d⁰ ferromagnetic K₂N monolayer with a high Curie temperature. *Phys. Rev. B* 102, 125118.
- Julies, B.A., Knoesen, D., Pretorius, R., and Adams, D. (1999). A study of the NiSi to NiSi₂ transition in the Ni-Si binary system. *Thin Solid Films* 347, 201–207.
- Kalamaras, C.M., and Efstratiou, A.M. (2013). Hydrogen production technologies: Current state and future developments. *Conf. Pap. Energy* 2013, 1–9.
- Kim, J., and Anderson, W.A. (2005). Spontaneous nickel monosilicide nanowire formation by metal induced growth. *Thin Solid Films* 483, 60–65.
- Kresse, G., and Joubert, D. (1999). From ultrasoft pseudopotentials to the projector augmented-wave method. *Phys. Rev. B* 59, 1758.
- Li, F.-Y., Luo, X., Dai, X., Yu, Y., Zhang, F., and Chen, G. (2016). Hybrid Weyl semimetal. *Phys. Rev. B* 94, 121105.
- Li, J., Ma, H., Xie, Q., Feng, S., Ullah, S., Li, R., Dong, J., Li, D., Li, Y., and Chen, X.-Q. (2018a). Topological quantum catalyst: Dirac nodal line states and a potential electrocatalyst of hydrogen evolution in the TiSi family. *Sci. China Mater.* 61, 23.
- Li, P.K., Zhu, J.G., Handoko, A.D., Zhang, R.F., Wang, H.T., Legut, D., Wen, X.D., Fu, Z.H., Seh, Z.W., and Zhang, Q.F. (2018b). High-throughput theoretical optimization of hydrogen evolution reaction on MXenes by transition metal modification. *J. Mater. Chem. A* 6, 4271–4278.
- Li, G., Fu, C., Shi, W., Jiao, L., Wu, J., Yang, Q., Saha, R., Kamminga, M.E., Srivastava, A.K., Liu, E., et al. (2019a). Dirac nodal Arc semimetal PtSn₄: an ideal platform for understanding surface properties and catalysis for hydrogen evolution. *Angew. Chem.* 131, 13241–13246.

Li, G., Xu, Q., Shi, W., Fu, C., Jiao, L., Kamminga, M.E., Yu, M., Tuysuz, H., Kumar, N., Süß, V., et al. (2019b). Surface states in bulk single crystal of topological semimetal $\text{Co}_3\text{Sn}_2\text{S}_2$ toward water oxidation. *Sci. Adv.* 5, eaaw9867.

Li, L., Zeng, J., Qin, W., Cui, P., and Zhang, Z. (2019c). Tuning the hydrogen activation reactivity on topological insulator heterostructures. *Nano Energy* 58, 40.

Lim, K.R.G., Handoko, A.D., Nemanic, S.K., Wyatt, B., Jiang, H.-Y., Tang, J.W., Anasori, B., and Seh, Z.W. (2020). Rational design of two-dimensional transition metal carbide/nitride (MXene) hybrids and nanocomposites for catalytic energy storage and conversion. *ACS Nano* 14, 10834–10864.

Ma, R., Lin, G., Zhou, Y., Liu, Q., Zhang, T., Shan, G., Yang, M., and Wang, J. (2019). A review of oxygen reduction mechanisms for metal-free carbon-based electrocatalysts. *NPJ Comput. Mater.* 5, 78.

Mahmood, J., Anjum, M.A.R., Shin, S.-H., Ahmad, I., Noh, H.-J., Kim, S.-J., Jeong, H.Y., Lee, J.S., and Baek, J.-B. (2018). Encapsulating Iridium Nanoparticles inside a 3D cage-like organic network as an efficient and durable catalyst for the hydrogen evolution reaction. *Adv. Mater.* 30, 1805606.

Meng, W., Liu, Y., Zhang, X., Dai, X., and Liu, G. (2020a). A nonsymmorphic-symmetry-protected hourglass Weyl node, hybrid Weyl node, nodal surface, and Dirac nodal line in Pd_2X ($\text{X} = \text{S}, \text{Se}$) compounds. *Phys. Chem. Chem. Phys.* 22, 22399–22407.

Meng, W., Zhang, X., He, T., Jin, L., Dai, X., Liu, Y., and Liu, G. (2020b). Ternary compound HfCuP : An excellent Weyl semimetal with the coexistence of type-I and type-II Weyl nodes. *J. Adv. Res.* 24, 523–528.

Meyer, B., Gottlieb, U., Laborde, O., Yang, H.S., Lasjaunias, J.C., Sulpice, A., and Madar, R. (1997). Intrinsic properties of NiSi. *J. Alloy Compd.* 262–263, 235–237.

Moore, J.E. (2010). The birth of topological insulators. *Nature* 464, 194–198.

Nørskov, J.K., Bligaard, T., Logadottir, A., Kitchin, J.R., Chen, J.G., Pandelov, S., and Stimming, U. (2005). Trends in the exchange current for hydrogen evolution. *J. Electrochem. Soc.* 152, J23–J26.

Nørskov, J.K., Bligaard, T., Logadottir, A., Kitchin, J.R., Chen, J.G., Pandelov, S., and Stimming, U. (2015). Trends in the exchange current for hydrogen evolution. *J. Electrochem. Soc.* 152, J23–J26.

Obama, B. (2017). The irreversible momentum of clean energy. *Science* 355, 126–129.

Osawa, A., and Okamoto, M. (1939). Epitaxial formation of a metastable hexagonal nickel-silicide. *Sci. Rep. Tohoku Univ. First Ser.* 27, 326.

Pauling, L., and Soldate, A.M. (1948). The nature of the bonds in the iron silicide, FeSi , and related crystals. *Acta Crystallogr.* 1, 212.

Perdew, J.P., Burke, K., and Ernzerhof, M. (1996). Generalized gradient approximation made simple. *Phys. Rev. Lett.* 77, 3865.

Qi, X.-L., and Zhang, S.-C. (2010). Topological insulators and superconductors. *Rev. Mod. Phys.* 83, 1057.

Rajamathi, C.R., Gupta, U., Kumar, N., Yang, H., Sun, Y., Süß, V., Shekhar, C., Schmidt, M., Blumtritt, H., Werner, P., et al. (2017). Weyl semimetals as hydrogen evolution catalysts. *Adv. Mater.* 29, 1606202.

Ren, Y., Qiao, Z., and Niu, Q. (2016). Topological phases in two-dimensional materials: A review. *Rep. Prog. Phys.* 79, 066501.

Seh, Z.W., Kibsgaard, J., Dickens, C.F., Chorkendorff, I., Nørskov, J.K., and Jaramillo, T.F. (2017). Combining theory and experiment in electrocatalysis: Insights into materials design. *Science* 355, eaad4998.

Sidorenko, S.I., Makogon, Y.N., Voloshko, S.M., Pavlova, O.P., Kotenko, I.E., Mogilatenko, A.V., and Beddies, G. (2008). Diffusion formation of silicide phases in $\text{Ni/Si}(001)$ nanodimensional film system. *Defect Diffus Forum* 280–281, 9–14.

Skúlasón, E., Karlberg, G.S., Rossmeisl, J., Bligaard, T., Greeley, J., Jónsson, H., and Nørskov, J.K. (2007). Density functional theory calculations for the hydrogen evolution reaction in an electrochemical double layer on the Pt(111) electrode. *Phys. Chem. Chem. Phys.* 9, 3241–3250.

Soluyanov, A.A., Gresch, D., Wang, Z., Wu, Q., Troyer, M., Dai, X., and Bernevig, B.A. (2015). Type-II Weyl semimetals. *Nature* 527, 495–498.

Tiwari, J.N., Sultan, S., Myung, C.W., Yoon, T., Li, N., Ha, M., Harzandi, A.M., Park, H.J., Kim, D.Y., Chandrasekaran, S.S., et al. (2018). Multicomponent electrocatalyst with ultralow Pt loading and high hydrogen evolution activity. *Nat. Energy*. 3, 773–782.

Toman, K. (1951). The structure of NiSi. *Acta Crystallogr.* 4, 462.

Turner, J.A. (2004). Sustainable hydrogen production. *Science* 305, 972–974.

Wan, X., Turner, A.M., Vishwanath, A., and Savrasov, S.Y. (2011). Topological semimetal and Fermi-arc surface states in the electronic structure of pyrochlore iridates. *Phys. Rev. B* 83, 205101.

Wang, L.R., Jin, L., Liu, G.D., Liu, Y., Dai, X.F., and Zhang, X.M. (2021a). Theoretical realization of two-dimensional Dirac/Weyl line-node and traversing edge states in penta- X_2Y monolayers. *Appl. Mater. Today* 23, 10105.

Wang, L.R., Zhang, X.M., Meng, W.Z., Liu, Y., Dai, X.F., and Liu, G.D. (2021b). A topological quantum catalyst: the case of two-dimensional traversing nodal line states associated with high

catalytic performance for the hydrogen evolution reaction. *J. Mater. Chem. A*. 9, 2245.

Wang, T., Jin, R., Wu, X., Zheng, J., Li, X., and Ostrikov, K. (2018). A highly efficient Ni-Mo bimetallic hydrogen evolution catalyst derived from a molybdate incorporated Ni-MOF. *J. Mater. Chem. A*. 6, 9228–9235.

Wang, X., Maeda, K., Thomas, A., Takanabe, K., Xin, G., Carlsson, J.M., Domen, K., and Antonietti, M. (2009). A metal-free polymeric photocatalyst for hydrogen production from water under visible light. *Nat. Mater.* 8, 76–80.

Weng, H., Liang, Y., Xu, Q., Yu, R., Fang, Z., Dai, X., and Kawazoe, Y. (2015). Topological node-line semimetal in three-dimensional graphene networks. *Phys. Rev. B*. 92, 045108.

Wood, I.G., Ahmed, J., Dobson, D.P., and Vocadlo, L. (2013). High-pressure phase transitions and equations of state in NiSi. III. A new high-pressure phase of NiSi. *J. Appl. Cryst.* 46, 14–24.

Wu, Q., Zhang, S., Song, H.-F., Troyer, M., and Soluyanov, A.A. (2018a). WannierTools: An open-source software package for novel topological materials. *Comput. Phys. Commun.* 224, 405.

Wu, W., Liu, Y., Li, S., Zhong, C., Yu, Z.-M., Sheng, X.-L., Zhao, Y.X., and Yang, S.A. (2018b). Nodal surface semimetals: Theory and material realization. *Phys. Rev. B*. 97, 115125.

Xiao, J., Kou, L., Yam, C.-Y., Frauenheim, T., and Yan, B. (2015). Toward rational design of catalysts supported on a topological insulator substrate. *ACS Catal.* 5, 7063–7067.

Xu, N., Wang, Z.W., Magrez, A., Bugnon, P., Berger, H., Matt, C.E., Strocov, V.N., Plumb, N.C., Radovic, M., Pomjakushina, E., et al. (2018). Evidence of a Coulomb -interaction-induced Lifshitz transition and robust hybrid Weyl semimetal in $\text{Td}-\text{MoTe}_2$. *Phys. Rev. Lett.* 121, 136401.

Xu, Y., Gu, Y., Zhang, T., Fang, C., Fang, Z., Sheng, X.-L., and Weng, H. (2019). Topological nodal lines and hybrid Weyl nodes in YCoC_2 . *APL Mater.* 7, 101109.

Yang, Q., Le, C., Li, G., Heineb, T., Felser, C., and Sun, Y. (2021). Enhancement of basal plane electrocatalytic hydrogen evolution activity via joint utilization of trivial and non-trivial surface states. *Appl. Mater. Today* 22, 100921.

Yang, S.A., Pan, H., and Zhang, F. (2014). Dirac and Weyl superconductors in three dimensions. *Phys. Rev. Lett.* 113, 046401.

Zhang, H., An, P., Zhou, W., Guan, B.Y., Zhang, P., Dong, J., and Lou, X.W.D. (2018a). Dynamic traction of lattice-confined platinum atoms into mesoporous carbon matrix for hydrogen evolution reaction. *Sci. Adv.* 4, eaao6657.

Zhang, M., Yang, Z., and Wang, G. (2018b). Coexistence of type-I and type-II Weyl points in the Weyl-semimetal OsC_2 . *J. Phys. Chem. C*. 122, 3533–3538.

STAR★METHODS

KEY RESOURCES TABLE

REAGENT or RESOURCE	SOURCE	IDENTIFIER
Software and algorithms		
VASP 5.4.1	Materials Design's MedeA software environment	https://www.vasp.at
WannierTools 2.5.1	Personally, by Quan sheng Wu et al.	http://www.wanniertools.com/

RESOURCE AVAILABILITY

Lead contact

Further information and requests for resources should be directed to and will be fulfilled by the lead contact, Xiaoming Zhang (zhangxiaoming87@hebut.edu.cn).

Materials availability

This study did not generate new unique materials.

Data and code availability

This article includes all datasets/code generated or analyzed during this study.

METHOD DETAILS

The work is performed under numerical calculations based on the density functional theory (DFT) (Blöchl, 1994), as realized via the Vienna ab initio simulation package (VASP) (Kresse and Joubert, 1999). As an inexpensive generalized gradient approximation (GGA), the exchange-related Potential- Burke-Ernzerhof (PBE) (Perdew et al., 1966) function is adopted in current work. The cutoff energy is set to be 500eV. For the calculations for electronic band structure of NiSi, the bulk Brillouin zone (BZ) is sampled with the k-mesh of 9 × 9 × 9 with the Γ point as the center. During calculation, the energy and force convergence standards are set to be 10^{-9} eV and 0.01 eV/ \AA^{-1} , respectively. The topologically surface status is calculated based on treatments as implemented in the WANNIERTOOLS package (Wu et al., 2018a, 2018b).

For the surface model for H adatom adsorption, we have tested slab thickness (n) by examining the surface energy dispersion with gradually increasing the number of n . The simulation shows the energy would show no dispersion with $n \geq 5$ during further add the slab thickness. Considering this, the surface model for NiSi is constructed by using a 10 unit-cell-thick slab ($n= 10$) with a 2 × 2 bottom supercell immobilized. In addition, during the simulation the DFT-D2 extension of Grimme is used to account for the long-range van der Waals interactions (Grimme, 2006). To explore the HER activity in NiSi compound, we calculate the value of ΔG_{H^*} following the formula (Nørskov et al., 2015):

$$\Delta G_{\text{H}^*} = \Delta E_{\text{H}} + \Delta E_{\text{ZPE}} - T\Delta S_{\text{H}} \quad (\text{Equation 1})$$

where ΔE_{H} is the adsorption energy of single H, ΔE_{ZPE} (ΔS_{H}) denotes the difference in zero-point energy (entropy) between the absorbed H and gaseous H.